Probing the barrier for $CH_2CHCO \rightarrow CH_2CH+CO$ by the velocity map imaging method

K.-C. Lau, Y. Liu, and L. J. Butler[a)]
The James Franck Institute and Department of Chemistry, The University of Chicago, Chicago, Illinois 60637

(Received 17 May 2005; accepted 16 June 2005; published online 10 August 2005)

This work determines the dissociation barrier height for $CH_2CHCO \rightarrow CH_2CH+CO$ using two-dimensional product velocity map imaging. The CH_2CHCO radical is prepared under collision-free conditions from C–Cl bond fission in the photodissociation of acryloyl chloride at 235 nm. The nascent CH_2CHCO radicals that do not dissociate to CH_2CH+CO, about 73% of all the radicals produced, are detected using 157-nm photoionization. The $Cl(^2P_{3/2})$ and $Cl(^2P_{1/2})$ atomic fragments, momentum matched to both the stable and unstable radicals, are detected state selectively by resonance-enhanced multiphoton ionization at 235 nm. By comparing the total translational energy release distribution $P(E_T)$ derived from the measured recoil velocities of the Cl atoms with that derived from the momentum-matched radical cophotofragments which do not dissociate, the energy threshold at which the CH_2CHCO radicals begin to dissociate is determined. Based on this energy threshold and conservation of energy, and using calculated C–Cl bond energies for the precursor to produce $CH_2C\dot{H}CO$ or $\dot{C}H_2CHCO$, respectively, we have determined the forward dissociation barriers for the radical to dissociate to vinyl+CO. The experimentally determined barrier for $CH_2C\dot{H}CO \rightarrow CH_2CH+CO$ is 21 ± 2 kcal mol^{-1}, and the computed energy difference between the $CH_2C\dot{H}CO$ and the $\dot{C}H_2CHCO$ forms of the radical gives the corresponding barrier for $\dot{C}H_2CHCO \rightarrow CH_2CH+CO$ to be 23 ± 2 kcal mol^{-1}. This experimental determination is compared with predictions from electronic structure methods, including coupled-cluster, density-functional, and composite Gaussian-3-based methods. The comparison shows that density-functional theory predicts too low an energy for the $\dot{C}H_2CHCO$ radical, and thus too high a barrier energy, whereas both the Gaussian-3 and the coupled-cluster methods yield predictions in good agreement with experiment. The experiment also shows that acryloyl chloride can be used as a photolytic precursor at 235 nm of thermodynamically stable $CH_2C\dot{H}CO$ radicals, most with an internal energy distribution ranging from ≈3 to ≈21 kcal mol^{-1}. We discuss the results with respect to the prior work on the $O(^3P)$+propargyl reaction and the analogous $O(^3P)$+allyl system. © *2005 American Institute of Physics*. [DOI: 10.1063/1.1995702]

I. INTRODUCTION

Polyatomic radical intermediates play an important role in a wide variety of elementary bimolecular reactions that proceed via addition or insertion mechanisms, including numerous reactions in combustion and atmospheric chemistry. This study investigates the acryloyl (or propenoyl) radical, the lowest-energy radical intermediate in the reaction of O atoms with propargyl radicals. The propargyl radical (C_3H_3) is a key species in the combustion of hydrocarbons.[1,2] Compared with other radical species, the propargyl radical has enhanced stability due to the delocalized electrons in the molecular frame.[3] This and the very large C–H bond energy of propargyl radicals compared to other unsaturated radicals, >90 kcal mol^{-1}, leads to a longer lifetime for the propargyl radical, allowing it to react with other species in the combustion flames.[4–7] One of these reactions, the subject of recent experimental and theoretical investigations, is the bimolecular collision between propargyl radical (C_3H_3) and atomic oxygen.[8–10]

Though the kinetics of the O+propargyl reaction has been investigated by Slagle *et al.*,[8] little is known about the product branching in this bimolecular reaction or the radical intermediates along the bimolecular reaction coordinates. Slagle *et al.*[8] used photoionization to detect possible reaction products, identifying H+propynal as a likely primary product channel. In recent crossed laser beam molecular-beam experiments of the O+propargyl reaction, Choi and coworkers used laser-induced fluorescence to detect the OH radical products from several possible $OH+C_3H_2$ product channels (where the channels produce C_3H_2 in different isomeric forms, including propargylene, vinylidenecarbene and cyclopropenylidene).[9,10] The apparatus used did not allow them to search for other product channels, but they calculated at the CBS-QB3 level of theory the energetics of several radical intermediates formed upon the addition of O atoms to propargyl radicals on the ground doublet surface to

a)Electronic mail: L-Butler@uchicago.edu

allow them to estimate possible product channel branching. Their theoretical results revealed that, in addition to the OH channels, two $H+C_3H_2O$ channels could contribute to the product branching. Indeed their Rice-Ramsperger-Kassel-Marcus (RRKM) statistical rate constants suggested that H +propynal should be the dominant product channel at the collision energies used in their experiment.[10] Very recently, however, Park *et al.*[11] also computationally investigated this potential-energy surface and identified another product channel for this reaction, the formation of vinyl radical $(CH_2CH)+CO$. This product channel is the most exothermic channel but had been missed as a possibility in the previous studies. The work of Park *et al.* indicated that the mechanism proceeds via several intermediate isomers en route to a low-energy $\dot{C}H_2CHCO$ radical. The $\dot{C}H_2CHCO$ radical intermediate then dissociates to form CH_2CH+CO:

$$\dot{C}H_2CHCO \rightarrow CH_2CH + CO. \quad (1)$$

That group is pursuing extensive trajectory studies on the O+propargyl reaction using a potential-energy surface calculated at the UB3LYP/6-311G(d,p) level of theory. We undertook the present experiments to provide an experimental benchmark for the energetics of the relevant transition states calculated for this chemical reaction, beginning here with the transition state for the dissociation of the propenoyl (or acryloyl), $CH_2CH\dot{C}O$, radical intermediate to vinyl +CO.

In order to determine the barrier energy to (1), one needs to prepare $CH_2CH\dot{C}O$ or $\dot{C}H_2CHCO$ radicals with internal energies ranging from below to above the barrier energy. In a previous photofragment translational spectroscopy experiment on the photodissociation of acryloyl chloride (CH_2 =CHCOCl) at 193 nm,[12] we were only able to generate energetically unstable $CH_2CH\dot{C}O$ radicals by the photolytic cleavage of the $CH_2CH(CO)-Cl$ bond at 193 nm.

$$CH_2CHCOCl \rightarrow CH_2CH\dot{C}O + Cl. \quad (2)$$

Measuring the velocities of the Cl atom cofragments determined that the propenoyl radicals formed had internal energies ranging from 23 to 68 kcal mol^{-1}, so even the lowest-internal-energy radicals were formed with energy higher than the dissociation barrier to CH_2CH and CO predicted at the G3//B3LYP level of theory. In other words, all nascent $CH_2CH\dot{C}O$ radicals underwent the secondary dissociation to vinyl+CO [reaction (1)]; those products were detected in the experiment. The results suggested an upper limit to the transition barrier for (1) to be 23 kcal mol^{-1}. Although this upper limit is in excellent agreement with the theoretical G3// B3LYP prediction[12] of 22.4 kcal mol^{-1}, it is somewhat lower than the UB3LYP barrier of 26.6 kcal/mol obtained by Park *et al.*,[11] and it is based on the negative result of not detecting any stable propenoyl radicals. Thus we undertook to experimentally determine the energy of the transition state barrier for (1), not just an upper limit, by generating $CH_2CH\dot{C}O$ radicals with internal energies both above and below the barrier.

In this study, we first photodissociate acryloyl chloride at 235 nm in order to produce a distribution of propenoyl radicals with internal energies low enough to extend below the predicted barrier for dissociation to vinyl+CO. This C–Cl bond photodissociation produces propenoyl radicals dispersed by velocity and, due to the conservation of energy, also by internal energy. On the basis of momentum and energy conservation, the center-of-mass recoil translational energy distribution $P(E_T)$ obtained from the kinetic-energy-release measurements of $CH_2CH\dot{C}O$ fragments would precisely match with that of the atomic Cl cofragments if none of the radicals underwent a dissociation to vinyl+CO. Since the propenoyl radicals with internal energy higher than the barrier height, formed from the C–Cl bond fission that release lower energies to recoil kinetic energy, can dissociate, the $P(E_T)$ measured from the surviving propenoyl radicals would show a cutoff at the energy threshold where the propenoyl radicals begin to dissociate in comparison with the $P(E_T)$ obtained from the Cl atom data. The energy threshold allows a quantitative determination of the transition state barrier associated in the dissociation reaction (1). In contrast to other methodologies which produce the radicals in a molecular-beam source (e.g., flash pyrolysis)[13] and access the dissociation channels of the radical by the UV excitation, our method of producing radicals with a distribution of internal energies spanning the barrier energy of interest, using the distribution of relative kinetic energies imparted in the precursor photodissociation, does not require the electronic excitation of the radical. Thus it offers a more direct probe of the radical's ground electronic state dissociation dynamics.

To make the comparison between the $P(E_T)$'s derived from velocity measurements of each of the momentum-matched photofragments possible, one must measure the total $P(E_T)$ appropriately summed over all quantum states of the photofragments. When the photofragments are probed by state-selective photoionization, one has to reconstruct the total $P(E_T)$ with line strength corrections, which are unknown for most polyatomic radical species. Thus, we use a nonstate-selective 157-nm photon source to photoionize all the $CH_2CH\dot{C}O$ fragments formed in the 235-nm photodissociation with equal efficiency. The ionization energy of the $CH_2CH\dot{C}O$ radical is near 7.0 eV,[14] which is accessible by a 157-nm F_2 excimer laser. The resulting $P(E_T)$ obtained should accurately represent the quantum yield weighted sum of the quantum-state-resolved $P(E_T)$'s if the photoionization cross section is independent of the internal energy of the radical for the population of nascent radicals. (Indeed, this requirement has recently been exploited by Aguirre and Pratt[15] to measure relative photoionization cross sections at 118 nm for the I $^2P_{1/2}$ vs the I $^2P_{3/2}$ products in the photodissociation of CH_3I and CF_3I, and by Lambert *et al.*[16] in their studies of the photodissociation of N_2O, using the 130-nm photoionization of the NO product to determine a branching between the two N atom+NO product channels.) In this work, we explicitly check this assumption by comparing the portion of the $P(E_T)$ at internal energies where the radical fragments are formed with internal energies stable to dissociate to vinyl+CO with the corresponding portion of

the $P(E_T)$ derived from the velocities measured for the Cl atom cofragments, as they must be related by momentum conservation. We took care with this because prior work on the photodissoviation of 2-chlorobutane by Gross *et al.*[17] showed that the 157-nm photoionization of the resulting *t*-butyl radical gave a total kinetic-energy-release distribution that differed by a couple kcal mol^{-1} from that derived from the Cl atom spectra. With careful signal averaging and calibrations, the present data did give $P(E_T)$'s from the $CH_2CH\dot{C}O$ and Cl fragments which are in very good agreement ($+/-0.5$ kcal mol^{-1}) with each other for energies that produce stable propenoyl radicals. The experiments were carried out with the two-dimensional photofragment velocity map imaging[18,19] apparatus in our laboratory at the University of Chicago.

One important goal of this and related works is to benchmark electronic structure predictions of transition states in chemical reactions. Many theoretical methods include an empirical correction determined from a set of experimental heats of formation of stable molecular and atomic species. There is much less data available to empirically correct or benchmark predictions for barrier heights, particularly in reactions involving radical species.[20] A recent work in our group has provided such data for the barriers associated with bimolecular and unimolecular reactions involving 2-propenyl,[21] 1-propenyl,[22] 1-buten-2-y1,[23] 2-buten-2-y1,[24] propionyl,[25] and vinoxy[26] radical intermediates. Currently, the Gaussian-3 (G3) theoretical procedure and its variants[27–29] are among the most popular quantum-chemical computation schemes for energetic calculations because of their high efficiency and accuracy. The G3 theory and its variants include a high-level correction determined empirically from a fit to a set of experimental data, including ionization energies, electron affinities and heats of formation of stable molecules. These electronic structure methods then give exceptional accuracy, to better than 1.5 kcal mol^{-1}, in predicting the thermochemistry of stable species.[30] However, it is important to benchmark the performance of these theoretical procedures in predicting barrier energies at the transition state of chemical reactions involving polyatomic radicals, as such transition states do not comprise the experimental data set used to define the empirical correction and as they are the key to chemical reaction rates. Finally, since the O+propargyl reaction is currently being studied by trajectory methods on a potential-energy surface at the UB3LYP level of theory, we seek an experimental determination of the relevant barrier heights to assess the importance of the G3 correction, which is relatively computationally expensive. In the view of the scarcity of accurate transition barrier heights for radical species, the comparison between the transition state barrier obtained here and the theoretical predictions serves as a key benchmark for these electronic structure methods.

II. EXPERIMENTAL AND THEORETICAL METHODS

A. Experiment

The experimental two-dimensional photofragment velocity map imaging apparatus has been described in detail previously.[31] Acryloyl chloride (with purity of 96%) was purchased from Aldrich and used without further purification. The acryloyl chloride sample was introduced into the photodissociation region in the form of a skimmed supersonic beam. The acryloyl chloride liquid sample (10%) was bubbled through by helium gas (90%) prior to the expansion through a room-temperature pulsed valve (nozzle diameter ≈ 0.6 mm) at a stagnation pressure of 500 Torr.

The 532-nm output of a pulsed injection-seeded neodymium:yttrium aluminum garnet (Nd:YAG) continuum laser was used to pump a dye laser (Lambda Physik, FL3002, LDS698 dye), generating visible radiation in the region of 675–715 nm. The dye laser output was frequency doubled in a potassium dihydrogen phosphate (KDP) crystal, and the resulting 353-nm light was mixed with the 706-nm fundamental in a beta-barium borate (BBO) crystal to produce the 235-nm photons. A focusing lens (focal length length ≈ 109 mm) was used to focus the 235-nm laser beam into the chamber. The 235-nm light is linearly polarized along an axis vertically perpendicular to the molecular beam and parallel to the detector surface. The parent acryloyl chloride molecules were dissociated by the 235-nm photons. The $Cl(^2P_{1/2})$ and $Cl(^2P_{3/2})$ fragments were ionized via [2+1] resonance-enhanced multiphoton ionization (REMPI) at 235.20 nm ($4p\ ^2P_{1/2} \leftarrow 3p\ ^2P_{1/2}$) and 235.34 nm ($4p\ ^2D_{3/2} \leftarrow 3p\ ^2P_{3/2}$), respectively.[32] A 157-nm F_2 excimer laser (EX10F/300) was used to ionize the $CH_2CH\dot{C}O$ fragments formed in the photodissociation of acryloyl chloride. The 157-nm laser was focused into the reaction chamber by a focusing lens (focal length ≈ 50 mm), and the light path outside the chamber was purged with nitrogen gas. During the experiment, the pulse energy of both the 157- and 235-nm lasers was carefully monitored to minimize the Coulomb repulsion between the ions formed in the photodissociation region.

The spherically expanding ion clouds formed in the photodissociation were accelerated toward a two-dimensional position-sensitive detector by an electrical ion lens assembly with a repeller/extractor voltage ratio of 1.404. After flying through the time-of-flight (TOF) drift region (≈ 577 mm), the ions were collected by a detector (Burle 3040FM) which consists of a chevron multichannel plate (MCP) coupled with a P20 phosphor screen by fiber optics. In order to detect only the ions of interest, the front plate of the MCP was pulsed to -750 V at the appropriate arrival time with a width of ≈ 70 ns. The phosphor screen was maintained at 3.5 kV above the potential of the rear MCP plate. Images appearing on the phosphor screen were recorded by a 1376×1040-pixel charge-coupled device camera (La Vision Imager 3) with a standard 35-mm camera lens. The ion signal was obtained with event counting,[33] using the algorithm in the DAVIS software, and each image was accumulated for over 100 000 laser shots. During the $Cl(^2P_{1/2})$ and $Cl(^2P_{3/2})$ fragment detection, the laser was scanned over the Doppler profile. The reconstruction of images to three-dimensional scattering distributions was performed using the Gaussian basis-set expansion Abel transformation method developed by Dribinski *et al.*[34]

The timing sequence for opening the pulsed valve, firing

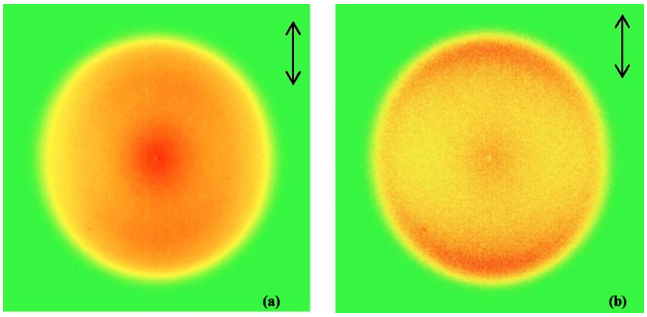

FIG. 1. (Color online) (a) Raw image of $Cl(^2P_{3/2})$ obtained by dissociating and probing with the same laser pulse at 235.34 nm via the $4p\ ^2D_{3/2} \leftarrow 3p\ ^2P_{3/2}$ transition. (b) Raw image of $Cl(^2P_{1/2})$ obtained by dissociating and probing with the same laser pulse at 235.20 nm via the $4p\ ^2P_{1/2} \leftarrow 3p\ ^2P_{1/2}$ transition. Laser polarization is shown by the arrow. Each raw image has a dimension of 861×861 pixels.

the Nd:YAG and F_2 excimer lasers, pulsing the MCP, and capturing the ion images were controlled by a digital pulse generator (Stanford Research DG535) at a repetition rate of 20 Hz.

B. Theoretical calculations

The $D_0(CH_2CH(CO)-Cl)$ and the transition state barrier heights involved in reaction (1) were calculated by the G3 (Ref. 27) and G3//B3LYP (Ref. 28) methods. We also evaluated the D_0 and the barrier heights at the coupled-cluster level with single and double excitations plus a quasiperturbative triple excitation [CCSD(T)] (Ref. 35) together with Dunning's correlation-consistent basis sets.[36] Specifically, the geometries of *cis-/trans*-$CH_2{=}CHCOCl$, the *cis-/trans*-$CH_2CH\dot{C}O$ and linear-$\dot{C}H_2CHCO$ (A'') radicals, CH_2CH, CO, and the *cis/trans* transition state (TS) structures were optimized at the CCSD(T)/6-311G(2*df*,*p*) level. Based on the optimized structures, single-point frozen-core energy calculations were carried out at the CCSD(T)/aug-cc-pV(Q+d)Z level of theory. Our results include a zero-point vibrational energy (ZPVE) correction at the minimum and transition state structures using the harmonic vibrational frequencies at the CCSD(T)/6-311G(2*df*,*p*) level. The core-valence electronic correlation (1*s* electrons on C and O, 2*s*/2*p* electrons on Cl) was obtained at the CCSD(T) level using an aug-cc-pwCVTZ basis set.[37] The G3 and G3//B3LYP calculations were performed with the GAUSSIAN03 package of programs[38] and all the CCSD(T) single-point energies and vibrational frequency calculations were done with the MOLPRO 2002.6 program.[39]

III. RESULTS AND DISCUSSION

A. Translational energy distributions

Raw images of the $Cl(^2P_{3/2})$ and $Cl(^2P_{1/2})$ photofragments are shown in Fig. 1 with the laser polarization direction in the vertical axis. The $Cl(^2P_{1/2})$ image indicates that there is an intense high-recoil-kinetic-energy component in the polar region while the $Cl(^2P_{3/2})$ image shows two weak velocity components of the Cl atom product, with a high-kinetic-energy component in the polar region of the image and a relatively lower kinetic-energy signal around the equatorial area. The speed distributions of the $Cl(^2P_{3/2})/Cl(^2P_{1/2})$ products are extracted by integrating the three-dimensional speed distributions over all solid angles at each velocity and the total $P(E_T)$ are derived from the $Cl(^2P_{3/2})/Cl(^2P_{1/2})$ atomic velocity distributions using the conservation of momentum and correcting with the appropriate Jacobian. (Such distributions are often called total-kinetic-energy-release (TKER) distributions in imaging studies, but we use here the more usual notation of $P(E_T)$ distributions as they have been defined in general for scattering studies.) The $P(E_T)$ distributions are displayed in Fig. 2. The $CH_2CHCO+Cl(^2P_{3/2})$ translational energy distribution evidences three components. The majority of the distribution is contributed from fast Cl atoms with recoil translational energies peaked at ≈ 23 kcal mol^{-1}. A shoulder in the region of 10–15 kcal mol^{-1} appears on the lower-translational-energy side of high-kinetic-energy C–Cl fission channel. There is another small broad component of low-translational-energy Cl atoms. The $CH_2CHCO+Cl(^2P_{1/2})$ translational energy distribution also evidences the two major components, but the lowest-kinetic-energy C–Cl bond fission channel does not result in detectable $Cl(^2P_{1/2})$ products. The highest- and lowest-kinetic-energy C–Cl bond fission channels in acryloyl chloride observed at 235 nm is similar to that at 193 nm. The mechanism for the highest-recoil-kinetic-energy C–Cl bond fission channels in acryloyl chloride is likely analogous to that for the C–Cl bond fission of other systems involving a $\pi \rightarrow \pi^*$ transition, such as allyl chloride[31,40] and propargyl chloride,[41] arising from electronic predissociation via a state repulsive along the C–Cl bond. The lowest-translational-energy channel and the intermediate shoulder results from the C–Cl fission, following more complicated mechanisms potentially involving internal conversion to the ground electronic state or intersystem crossing and production of the radical cofragment in an excited electronic state. Interestingly, the C–Cl bond fission via the lowest-recoil-kinetic-energy mechanism only produces Cl atoms in the $Cl(^2P_{3/2})$

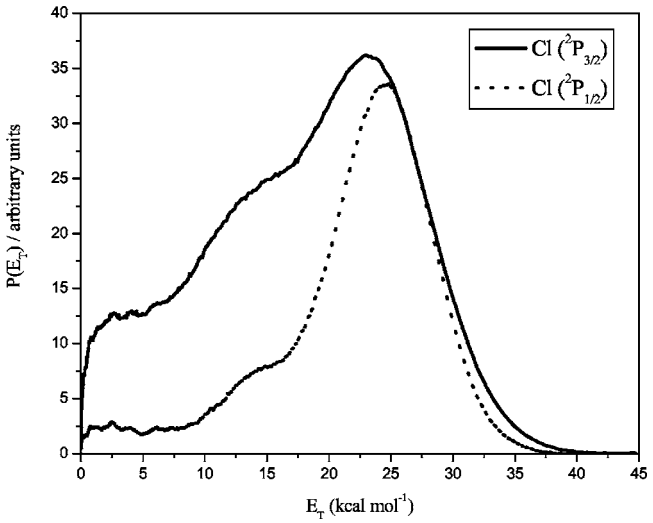

FIG. 2. Total center-of-mass translational energy distributions derived from Fig. 1. The distribution profiles for $CH_2CHCO+Cl(^2P_{3/2})$ and $CH_2CHCO+Cl(^2P_{1/2})$ are shown in solid and dotted lines, respectively.

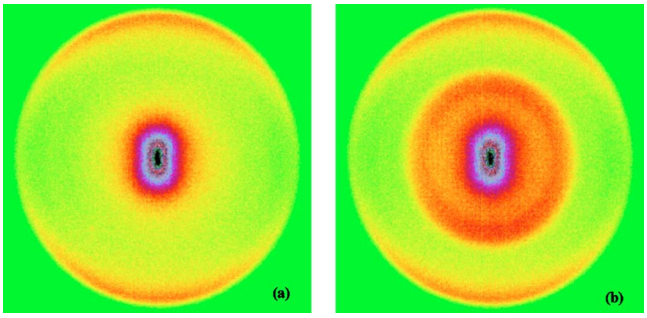

FIG. 3. (Color online) Raw images of the CH_2CHCO fragments obtained at (a) 157 nm and (b) 157+235 nm. An inner distribution appearing in (b) but not in (a) reveals that there is a contribution of CH_2CHCO fragments from 235 nm photodissociation with the radicals ionized by the 157-nm photons. Each image has a dimension of 861×861 pixels.

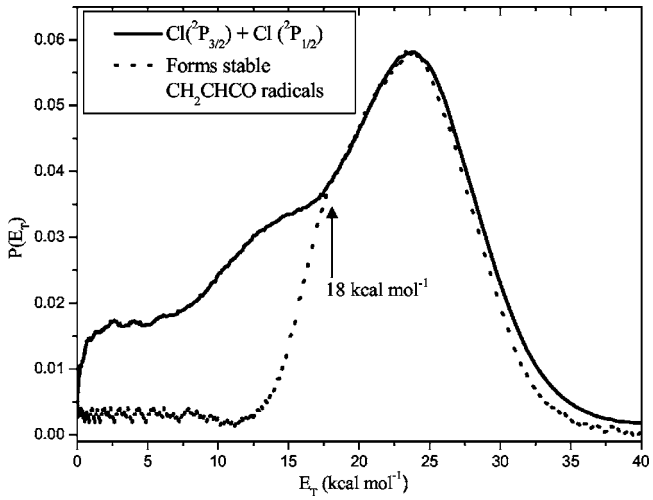

FIG. 4. Total center-of-mass translational energy distribution for the C–Cl bond fission and the portion of the distribution that results in stable radicals. The total center-of-mass translational energy distribution, obtained from the weighted sum of the individual Cl distributions in Figs. 1(a) and 1(b), is shown in solid line. The dotted-line distribution, corresponding to the 235-nm photodissociation events that from stable radicals, is derived from Figs. 3(a) and 3(b) after subtraction.

state; the same is true of the lowest-kinetic-energy C–Cl bond fission channel in allyl chloride[31] and propargyl chloride.[41]

The raw images of CH_2CHCO photofragments taken at 157 and 157+235 nm are displayed in Figs. 3(a) and 3(b), respectively. Both the 157- and the 235-nm light can photodissociate the acryloyl chloride molecules, but only the 157-nm photons are energetic enough to ionize the CH_2CHCO fragments. Due to the significant lower-kinetic-energy release from the CH_2CHCO fragments formed in the 235-nm photodissociation, it is possible to discriminate the CH_2CHCO radicals formed in 235 nm from those in the 157-nm photodissociation. As seen in Figs. 3(a) and 3(b), a high-recoil-kinetic-energy CH_2CHCO component is found in the polar region of both images, corresponding to the CH_2CHCO radical fragments formed in the 157-nm photodissociation. At the inner region of images in Fig. 3(b), an intense component due to the CH_2CHCO radicals formed in the 235-nm photodissociation is observed. The center of both images show that there are some low-kinetic-energy CH_2CHCO ion fragments, but these signals are well separated from the CH_2CHCO radicals formed at 235 nm. The $P(E_T)$ distribution for the CH_2CHCO radicals given in Fig. 4 is obtained by subtracting the $P(E_T)$ distribution at 157 nm from the $P(E_T)$ distribution at 157+235 nm. This is done prior to the normalization of the distributions, so there are no adjustable parameters in this subtraction. Thus the stable radical products produced in only the 235-nm photodissociation are unambiguously identified. They resulted from the C–Cl bond fission events characterized by a recoil translational energy distribution that ranges from ≈ 12 to ≈ 36 kcal mol^{-1} with a peak translational energy of about 23 kcal mol^{-1}. The radicals, detected by the 157-nm photoionization, in this distribution are stable to dissociate to vinyl+CO by virtue of the higher recoil kinetic energy in the C–Cl bond fission events that formed them; they are left with a lower internal energy, so they have a lower vibrational energy than the barrier to reaction (1). We use this in the next two sections to determine the forward energy barrier to reaction (1). Note that the stable radicals we detect have, by energy and momentum conservation, internal energies ranging from ≈ 5 to about 29 kcal mol^{-1} (relative to the zero-point level of the minimum-energy radical structure) and that starting at 18 kcal mol^{-1} in ET some of the radicals are clearly lost to dissociation. Radicals with a total internal energy that is higher than the dissociation barrier will be stable to dissociate to vinyl+CO if a significant fraction of the internal energy has been partitioned to the rotation of the radical. Conservation of angular momentum prevents the dissociation of those radicals.

B. Comparison between the $P(E_T)$'s derived from the Cl and the stable CH_2CHCO products

The CH_2CHCO fragments recoil from both Cl($^2P_{3/2}$) and Cl($^2P_{1/2}$) atoms during the photodissociation process of acryloyl chloride, so the total C–Cl bond fission $P(E_T)$ should be constructed by summing the C–Cl bond fission $P(E_T)$'s derived from the individual Cl($^2P_{3/2}$) and Cl($^2P_{1/2}$) fragments weighted by the cross section for each channel. Since the Cl($^2P_{3/2}$) and Cl($^2P_{1/2}$) atoms are probed at very similar one-color REMPI wavelengths with the same laser power, the influence of photolysis and ionization photon intensity on the weighting factor can be ruled out. The slight difference between photodissociation cross sections at these wavelengths can also be neglected. The relative REMPI detection efficiencies,[42–46] however, must be taken into account. The relative line strengths for the $4p\ ^2P_{1/2} \leftarrow 3p\ ^2P_{1/2}$ and $4p\ ^2D_{3/2} \leftarrow 3p\ ^2P_{3/2}$ transitions have been determined to be 0.85 ± 0.10 by Liyanage *et al.*[42] The apparent cross sections for forming Cl($^2P_{3/2}$) and Cl($^2P_{1/2}$) before application of the line strength correction is obtained by integrating the ion signal intensity over the entire velocity range of the Cl images; then one scales this ratio by the relative line strength to get the relative cross section for each product channel. The Cl($^2P_{3/2}$) to Cl($^2P_{1/2}$) ion signal intensity ratio is determined from integrating our data to be 3.56:1. Dividing by the Liyanage line strength ratio to correct this ratio of apparent cross sections for the larger sensitivity to Cl($^2P_{1/2}$) gives a branch-

ing ratio of 4.19:1 for the C–Cl fission events producing $Cl(^2P_{3/2})$ to the C–Cl fission events producing $Cl(^2P_{1/2})$. Thus 81% of the C–Cl bond fissions produce $Cl(^2P_{3/2})$ and 19% of the C–Cl bond fission events produce $Cl(^2P_{1/2})$. To obtain a total $P(E_T)$ distribution for production of all CH_2CHCO radicals, we first normalize the $P(E_T)$'s for the production of each Cl spin-orbit state shown in Fig. 2 then calculate the weighted sum of these $P(E_T)$'s, 0.81 [$P(E_T)$ for producing $Cl(^2P_{3/2})$] +0.19 [$P(E_T)$ for producing $Cl(^2P_{1/2})$].

The $P(E_T)$ distribution thus obtained for all C–Cl fission events, both those that produce stable radical cofragments and those that produce unstable radical cofragments to the Cl atoms, is shown in Fig. 4 in the solid line. The velocity distribution of the stable radicals detected upon the 235-nm photodissociation of acrolyl chloride (derived from the images in Fig. 3 and described in the prior section) allows us to determine the portion of the $P(E_T)$ distribution which resulted in Cl atoms+stable radicals. This experimental result is shown in the dotted-line $P(E_T)$ distribution in Fig. 4, labeled "forms stable CH_2CHCO radicals." Clearly, the CH_2CHCO radicals from the C–Cl bond fission events, partitioning less energy to recoil kinetic energy, were left with sufficient internal vibrational energy to overcome the energetic barrier to dissociate to vinyl+CO; hence these fragments do not contribute to the dotted-line $P(E_T)$ distribution. The highest recoil kinetic energy that produces radicals with enough internal energy to surmount the barrier and dissociate to vinyl+CO is thus simply determined by comparing the two distributions in Fig. 4. As shown in Fig. 4, the $P(E_T)$ profile of the CH_2CHCO fragments is almost perfectly matched with that of the Cl fragments for the high recoil kinetic energies. (There is a slight deviation between the two $P(E_T)$'s in the high-energy tail, presumably from difficulties with background subtraction). At the total translational energy of 18 ± 1 kcal mol^{-1}, the $P(E_T)$ derived from the stable CH_2CHCO fragments begins to drop below the total $P(E_T)$ for the C–Cl bond fission (derived from the Cl atom data), producing both stable and unstable radical species. Thus it is at the threshold recoil kinetic energy of 18 ± 1 kcal mol^{-1} that some of the radicals are produced with just enough internal energy to dissociate to vinyl+CO. Clearly, at that threshold recoil kinetic energy the dissociative radicals would be produced in coincidence with the lower-spin-orbit-state Cl atoms, as radicals produced in coincidence with $Cl(^2P_{1/2})$ with this same recoil kinetic energy would have a 2.5-kcal mol^{-1} lower internal energy. Thus, it was essential for an accurate determination of the barrier energy to have determined that at least some $Cl(^2P_{3/2})$ is formed in the C–Cl bond fission events that partition 18 kcal mol^{-1} to relative kinetic energy. (Note also that to be detected as a "stable" radical, the radical must not dissociate before being ionized by the 157-nm light and travel as parent ion to the detector, as the mass is selected by the MCP time gating.)

C. Dissociation barrier for $\dot{C}H_2CHCO \rightarrow CH_2CH+CO$

The theoretical $D_0(CH_2CH(CO)-Cl)$ and barrier height for the transition state (TS) in the dissociation (1) are listed in Table I. There are two conformers (*cis* and *trans*) for acryloyl chloride. All three theoretical methods predict that the relative stability of both conformers differs by less than 0.5 kcal mol^{-1}. Thus, both conformers are indistinguishable, given the experimental uncertainty in this study and the accuracy of the theoretical methods employed here. As found by Cooksy,[47] there are three possible conformers for CH_2CHCO radicals: *cis*-$CH_2CH\dot{C}O$, *trans*-$CH_2CH\dot{C}O$ and linear-$\dot{C}H_2CHCO$. The *cis*- and *trans*-$CH_2CH\dot{C}O$ conformers have the carbonyl groups in the *cis* and *trans* configurations with respect to the CH_2CH, while the linear-$\dot{C}H_2CHCO$ has an almost linear CCO skeleton and a different dominant electronic configuration at the minimum-energy structure. Both the *trans*-$CH_2CH\dot{C}O$ and the linear-$\dot{C}H_2CHCO$ conformers are found to have planar C_s symmetry, and the *cis*-$CH_2CH\dot{C}O$ has C_1 symmetry. At the G3 and CCSD(T) levels of theory, the linear-$\dot{C}H_2CHCO$ is found to be more stable than the *cis*- and *trans*-$CH_2CH\dot{C}O$ conformers. However, the *trans*-$CH_2CH\dot{C}O$ conformer is the most stable structure at the G3||B3LYP level. The difference between the G3 and G3//B3LYP theories is that the regular G3 theory is based on the optimized geometry at the MP2(full)/6-31G(*d*) while the latter is based on geometry at the B3LYP/6-31G(*d*) level. Upon careful examination, it is found that the B3LYP/6-31G(*d*) optimized structure of the *trans*-$CH_2CH\dot{C}O$ conformer is significantly more stable than that of the linear-$CH_2CH\dot{C}O$ conformer in the QCISD(T)/6-31G(*d*) single-point energy calculation of the G3//B3LYP procedure. However, there is less difference in stability between the MP2(full)/6-31G(*d*) optimized structure of the *trans*-$CH_2CH\dot{C}O$ and the linear-$\dot{C}H_2CHCO$ conformers in the same single-point energy calculation of the G3 procedure. As pointed out by Cooksy,[47] the potential along the torsional coordinate to transform between these three CH_2CHCO radical conformers is extremely flat and the barriers are on the order of a few kcal mol^{-1}. It is not surprising to find that the conformation and the relative stability of the

TABLE I. Theoretical $D_0(CH_2CH(CO)-Cl)$ and barrier height for (1) in kcal mol^{-1}. (The D_0 and barrier height calculations correspond to reactions where *cis*- or *trans*-$CH_2{=}CH(CO)Cl$ is dissociated into linear-$\dot{C}H_2CHCO+Cl$ and the linear-$\dot{C}H_2CHCO$ radical undergoes dissociation to form CH_2CH and CO via the *cis*- or *trans*-TS, respectively. The G3//B3LYP results in this table also refer to the linear-$\dot{C}H_2CHCO$ radical intermediate for consistency, though the *trans* conformer is predicted to have the minimum energy at that level of theory. The predicted barrier from the *trans* conformer is given in Ref. 12.)

	G3	G3//B3LYP	CCSD(T)[a]
D_0(*cis*-$CH_2CH(CO)$-Cl)	81.8	81.9	82.2
D_0(*trans*-$CH_2CH(CO)$-Cl)	82.2	82.2	81.9
Barrier height (*cis*-TS)	24.6	21.9	23.5[b]
Barrier height (*trans*-TS)	24.5	22.0	23.6[b]

[a]Based on the CCSD(T)/6-311G(2*df*,*p*) optimized geometries, single-point energies were calculated at the CCSD(T)/aug-cc-pV(Q+d)Z level of theory. Zero-point vibrational energy correction and core-valence electronic correlations were included (see text).
[b]The respective barrier heights based on the B3LYP/6-311G(2*df*,*p*) optimized geometries of *cis*-TS and *trans*-TS are 23.1 and 23.2 kcal mol^{-1}.

TABLE II. Theoretical $CH_2CH\cdots CO$ bond distance (in angstrom) at the *trans*-TS and *cis*-TS obtained at different levels of theory.

$CH_2CH\cdots CO$	MP2/6-311G(2*df*,*p*)	B3LYP/6-311G(2*df*,*p*)	CCSD(T)/6-311G(2*df*,*p*)
trans-TS	2.191	2.433	2.233
cis-TS	2.187	2.421	2.238

CH_2CHCO radicals are very sensitive to the basis sets and the theoretical methods employed. In spite of this, the stability differences among these three CH_2CHCO conformers are about 1.5 kcal mol^{-1} at both the G3 and G3//B3LYP levels and about 2 kcal mol^{-1} at the CCSD(T) level of theory. Since the linear-$\dot{C}H_2CHCO$ conformer is found to be the most stable at the CCSD(T) level, its energy is taken as the global minimum of the CH_2CHCO conformers and it is used for the bond energy and barrier height evaluations in Table I. (Note that for consistency we thus list energies with respect to the zero-point level for this structure even for the G3//B3LYP results in Table I, even though at that level of theory it is not the most stable conformer.)

The calculated D_0 for *cis-/trans*-$CH_2{=}CH(CO)Cl$ reported in Table I (and used in the barrier height determination) is for dissociation to form the linear-$\dot{C}H_2CHCO$ radical structure and a $Cl(^2P_{3/2})$ atom. In the actual dynamics, however, the *trans*-$CH_2CH\dot{C}O$, *cis*-$CH_2CH\dot{C}O$, and linear-$\dot{C}H_2CHCO$ radicals could each be formed and could interconvert on the time scale of the dissociation dynamics. Predicted by the three methods, both the D_0(*cis*-$CH_2CH(CO)-Cl$) and D_0(*trans*-$CH_2CH(CO)-Cl$) are very similar. Because the experimental heats of formation for the $CH_2{=}CHCOCl$ and CH_2CHCO species are not known and the calculated $D_0(CH_2CH(CO)-Cl)$ agree well for the theoretical methods, the calculated D_0 are our best estimate of the C–Cl bond dissociation energy. The barrier heights in Table I were calculated for the linear-$\dot{C}H_2CHCO$ radicals undergoing dissociation to form CH_2CH and CO via the respective *cis* and *trans* transition states. The dissociation barrier heights for the linear-$\dot{C}H_2CHCO$ radical via the *cis* and *trans* transition states predicted by all three theoretical methods are almost identical. Thus, the barrier heights for the dissociation channels via either the *cis* transition state or the *trans* transition state are expected to be indistinguishable. The bond distance between the CH_2CH and CO moieties is the main degree of freedom involved in the dissociation of the CH_2CHCO radical on the potential-energy surface. The $C\cdots CO$ bond distance at the *cis* and the *trans* transition states are listed in Table II. At the MP2/6-311G(2*df*,*p*) and CCSD(*T*)/6-311G(2*df*,*p*) levels, the $CH_2CH\cdots CO$ distance in both transition states are $\approx$2.19 and $\approx$2.23 Å, respectively. The distances predicted for both transition states at the B3LYP/6-311G(2*df*,*p*) level are significantly longer by $\approx$0.2 Å; this implies that the density-functional theory (DFT) method predicts a loose transition state structure compared with the MP2 and CCSD(T) methods. However, the barrier heights calculated at the CCSD(T)/cc-pV(Q+d)Z level using the B3LYP/6-311G(2*df*,*p*) optimized geometry are only slightly lower than that based on the CCSD(T)/6-311G(2*df*,*p*) geometry by 0.4 kcal mol^{-1} (see footnote "b" in Table I). The difference in the transition state geometry here has little effect on the theoretically predicted barrier height. All the optimized CCSD(T) structures, vibrational frequencies, and moments of inertia are given in the EPAPS supplementary information[48] attached to this paper.

The detailed dissociation mechanism for the CH_2CHCO radical to vinyl+CO on the potential-energy surface is complicated by the three possible conformers of CH_2CHCO radicals which could be formed by the photodissociation of two possible conformers of acryloyl chloride and the fact that the dissociation to vinyl+CO could proceed via two possible transition state structures. If the *trans-/cis*-CH_2CHCO conformers are generated from the 235-nm photodissociation of the corresponding conformers of acryloyl chloride, some of the *trans-/cis*-$CH_2CH\dot{C}O$ radicals could convert to the energetically low-lying linear-$\dot{C}H_2CHCO$ conformer. The linear-$\dot{C}H_2CHCO$ conformer has A'' symmetry at its minimum-energy structure, so to access the A' *cis-/trans*-transition state structures en route to the vinyl+CO products the system must traverse a conical intersection. Thus electronically nonadiabatic effects may be important along the reaction coordinate.

We can derive the internal energy $[E_{int}(\dot{C}H_2CHCO)]$ of the CH_2CHCO fragments (the internal energy with respect to the zero-point level of the CCSD(T) predicted minimum-energy structure) formed upon the C–Cl bond fission in the 235-nm photodissociation of acryloyl chloride from conservation of energy:

$$E_{int}(\dot{C}H_2CHCO) = E_{int}(CH_2{=}CHCOCl) + h\nu - D_0(CH_2CH(CO)-Cl) - E_T - E_{int}(Cl(^2P_{3/2})) \text{ or } E_{int}(Cl(^2P_{1/2})), \quad (3)$$

where $h\nu$ is equal to 121.6 kcal mol^{-1} (or 121.5 for the alternate wavelength used). The $E_{int}(Cl(^2P_{3/2}))$ and $E_{int}(Cl(^2P_{1/2}))$ are zero and 2.5 kcal mol^{-1}, respectively, the splitting between the ground spin-orbit state $(^2P_{3/2})$ and excited spin-orbit state $(^2P_{1/2})$ of the Cl atom. The average internal energy content of acryloyl chloride (i.e., $E_{int}(CH_2{=}CHCOCl)$) at 298 K is estimated to be 1.5 kcal mol^{-1} using the vibrational frequencies calculated at the CCSD(T)/6-311G(2*df*,*p*) level and assuming that rotation cools effectively in the He-seeded expansion but that vibration does not. For the radicals formed from dissociation events partitioning 18 ± 1 kcal mol^{-1} to relative kinetic energy, the highest recoil kinetic energy that produces dissociative radicals, the dissociative radicals would be formed in coincidence with

ground-spin-orbit-state Cl atoms. Thus we can use Eq. (3) with $E_{int}(Cl(^2P_{3/2}))=0$ to calculate the internal energy of these threshold radicals. Using the calculated CCSD(T) $D_0(CH_2CH(CO)-Cl)$ of 82 kcal mol^{-1}, this yields a value of 23 ± 2 kcal mol^{-1} for $E_{int}(\dot{C}H_2CHCO)$. This value represents the minimum internal energy at which the $\dot{C}H_2CHCO$ radicals is observed to be lost in the dissociation. Thus, the dissociation barrier height for the $\dot{C}H_2CHCO$ radicals to form the CH_2CH and CO molecules is estimated to be 23 ± 2 kcal mol^{-1}, which is in very good agreement with the G3 and CCSD(T) theoretical predictions. (This analysis assumes that a non-negligible fraction of the C–Cl bond fission events releasing 18 kcal/mol to relative kinetic-energy partitions little energy to the rotation of the radical. Assuming that the recoil velocity vector is along the C–Cl bond direction at the equilibrium ground-state geometry of acryloyl chloride, the resulting impact parameter is small, partitioning only 1.5 kcal mol^{-1} into the rotational energy of the radical for the *cis* conformer and 0.75 kcal mol^{-1} into the rotation for the *trans* conformer at a recoil kinetic energy of 18 kcal mol^{-1}. Thus the assumption that some radicals are formed with very little energy in rotation at this recoil energy is reasonable). $CH_2CH\dot{C}O$ radicals with an internal energy of 21 ± 2 kcal mol^{-1} could access the same vinyl+CO transition states and would exhibit the same E_T threshold of 18 ± 1 kcal mol^{-1} that we observe experimentally.

Note that our barrier energy determination depends on a conservation of energy expression that includes the C–Cl bond energy of acryloyl chloride, which is also obtained computationally at the same level of theory. The experiment ultimately only determines the sum of D_0 and the barrier height. Thus the uncertainty of 2 kcal mol^{-1} takes into account a few factors: the slight difference in D_0 from the *cis* and *trans* conformers of acryloyl chloride parent molecules, the extent of the vibrational relaxation of the molecular beam, and the uncertainty in the theoretical CCSD(T) $D_0(CH_2{=}CH(CO)-Cl)$ value. It is noted that the mean vibrational energy of acryloyl chloride drops to 0.3 kcal mol^{-1} at a vibrational temperature of 150 K. In our experience, the calculated D_0 at the CCSD(T)/aug-cc-pV(Q+d)Z level with the inclusion of harmonic ZPVE and core-valence correlation effects here has an uncertainty of about 1 kcal mol^{-1}.

This work and the prior experimental work in our group by Szpunar *et al.*,[12] which detected the vinyl+CO products from the CH_2CHCO radical, show that if the O+propargyl collision complex accesses the CH_2CHCO radical intermediate the barrier to the dissociation to vinyl+CO is low and thus vinyl+CO products should contribute significantly to the product branching. Inspection of the Park *et al.*[11] potential-energy surface reveals an energetically favorable path to producing this radical intermediate in the O+propargyl reaction, where the O atom addition at the end carbon atom of propargyl with a single H atom produces an $OCHCCH_2$ radical intermediate that is predicted to have a much lower barrier for isomerization to the CH_2CHCO radical than for dissociation to propynal+H. At the higher energies accessed in the bimolecular collision the propynal+H product channel could contribute significantly as entropic factors favor that channel. Surprisingly, the early photoionization mass spectrometry investigation of the O+propargyl reaction by Slagle *et al.*[8] did not identify any branching to the CO+vinyl product channel; they report that only the propynal signal is tentatively consistent with a primary product channel. Though the photoionization energies used in that work are too low to detect CO products, both the vinyl product and any acetylene produced from the unimolecular decomposition of the vibrationally hot vinyl radicals formed in this highly exothermic channel could have been detected. Slagle *et al.* noted that the acetylene signal observed did not have a rise-time profile consistent with the time decay of the reactants, so they attributed that signal to secondary collisions in the bulk experiments.[8] Further work to experimentally characterize the product branching is thus warranted. Calculations[49] on the analogous O+allyl reaction also reveal a path to a corresponding highly exothermic ethyl+CO product channel, but this product channel has also not been investigated experimentally, though H,[50] OH,[51] and acrolein[52] primary products have been detected.

IV. CONCLUSION

The barrier height for the dissociation of CH_2CHCO into CH_2CH and CO has been measured by two-dimensional product velocity map imaging. The photodissociation of acryloyl chloride at 235 nm produces a large fraction of nascent stable $CH_2CH\dot{C}O$ radicals, most with internal energy ranging from ≈3 to ≈21 kcal mol^{-1}, and a small fraction of dissociative radicals. By comparing the $P(E_T)$ obtained from the Cl cofragments of both the stable and unstable radicals with the portion of the $P(E_T)$ derived from the stable CH_2CHCO cofragments, we determine that the highest recoil translational energy that produces dissociative radicals is 18 ± 1 kcal mol^{-1}. Based on this kinetic-energy threshold and the conservation of energy, we have derived a forward transition state barrier height for $\dot{C}H_2CHCO\rightarrow CH_2CH$ and CO to be 23 ± 2 kcal mol^{-1}, the barrier height from the predicted lowest-energy structure of the radical. The experimental barrier height is in very good accord with the high-level *ab initio* theoretical predictions, though somewhat lower than the barrier predicted at the UB3LYP level of theory used to develop the potential-energy surface[11] in the ongoing trajectory calculations for the O+propargyl reaction. Though the calculated branching to the highly exothermic CO+vinyl channel should be minimally affected by using the less accurate barrier, this study indicates the importance of benchmarking some of the other barriers in the O+propargyl reaction, such as the one between the $HCCCH_2O$ radical intermediate and the H+propynal product channel. Efforts in our group to experimentally determine that barrier are ongoing.

ACKNOWLEDGMENTS

This work was supported by the Chemical, Geosciences, and Biosciences Division, Office of Basic Energy Sciences, Office of Science, U.S. Department of Energy, under Grant No. DE-FG02-92ER14305. The calculations in this work were performed using the Molecular Science Computing Fa-

cility (MSCF) in the William R. Wiley Environmental Molecular Sciences Laboratory, a national scientific user facility sponsored by the U.S. Department of Energy's Office of Biological and Environmental Research. Part of the calculations in this work used resources of the National Energy Research Scientific Computing Center, which is supported by the Office of Science of the U.S. Department of Energy under Contract No. DE-AC03-76SF00098.

[1] N. M. Marinov, M. J. Castaldi, C. F. Melius, and W. Tsang, Combust. Sci. Technol. **128**, 295 (1997).
[2] J. A. Miller and C. F. Melius, Combust. Flame **91**, 21 (1992).
[3] E. B. Jochnowitz, X. Zhang, M. R. Nimlos, M. E. Varner, J. F. Stanton, and G. B. Ellison, J. Phys. Chem. A **109**, 3812 (2005).
[4] J. A. Miller, Proc. Combust. Inst. **20**, 461 (1996).
[5] H. Richter and J. B. Howard, Prog. Energy Combust. Sci. **26**, 565 (2000).
[6] C. F. Melius, J. A. Miller, and E. M. Evleth, Proc. Combust. Inst. **24**, 621 (1992).
[7] D. K. Hahn, S. J. Klippenstein, and J. A. Miller, Faraday Discuss. **119**, 79 (2001).
[8] I. R. Slagle, G. W. Gmurczyk, L. Batt, and D. Gutman, Symp. Int. Combust. Proc. 23, 115 (1991).
[9] H. Lee, S.-K. Joo, L.-K. Kwon, and J.-H. Choi, J. Chem. Phys. **119**, 9337 (2003).
[10] H. Lee, S.-K. Joo, L.-K. Kwon, and J.-H. Choi, J. Chem. Phys. **120**, 2215 (2004).
[11] S. C. Park, B. Braams, and J. Bowman, J. Theor. Comput. Chem. **4**, 163 (2005).
[12] D. E. Szpunar, J. L. Miller, L. J. Butler, and F. Qi, J. Chem. Phys. **120**, 4223 (2004).
[13] I. Fischer, Int. J. Mass. Spectrom. **216**, 131 (2002).
[14] The G3//B3LYP prediction for the ionization energies of the three low-energy CH_2CHCO radicals are 6.87, 6.93, and 6.95 eV, and the value listed in the NIST Chemistry Webbook (http://webbook.nist.gov) is 7.0 eV.
[15] F. Aguirre and S. T. Pratt, J. Chem. Phys. (in press).
[16] H. M. Lambert, E. W. Davis, O. Tokel, A. A. Dixit, and P. L. Houston, J. Chem. Phys. **122**, 174304 (2005).
[17] R. L. Gross, X. Liu, and A. G. Suits, Chem. Phys. Lett. **362**, 229 (2002).
[18] A. J. R. Heck and D. W. Chandler, Annu. Rev. Phys. Chem. **46**, 335 (1995).
[19] A. T. J. B. Eppink and D. H. Parker, Rev. Sci. Instrum. **68**, 3477 (1997).
[20] See, for example, the determination of the barrier to the dissociation of the C_2H_2Cl radical to $Cl+C_2H_2$ in D. A. Blank, W. Sun, A. G. Suits, Y. T. Lee, S. W. North, and G. E. Hall, J. Chem. Phys. **108**, 5414 (1998).
[21] (a) J. A. Mueller, J. L. Miller, L. J. Butler, F. Qi, O. Sorkhabi, and A. G. Suits, J. Phys. Chem. A **104**, 11261 (2000); (b) J. A. Mueller, B. F. Parsons, L. J. Butler, F. Qi, O. Sorkhabi, and A. G. Suits, J. Chem. Phys. **114**, 4505 (2001).
[22] M. L. Morton, J. L. Miller, L. J. Butler, and F. Qi, J. Phys. Chem. A **106**, 10831 (2002). J. L. Miller, M. L. Morton, L. J. Butler, F. Qi, M. J. Krisch, and J. Shu, J. Phys. Chem. A **106**, 10965 (2002).
[23] J. L. Miller, M. J. Krisch, L. J. Butler, and J. Shu, J. Phys. Chem. A **109**, 4038 (2005).
[24] L. R. McCunn, M. J. Krisch, Y. Lui, L. J. Butler, and J. Shu J. Phys. Chem. A **109**, 6430 (2005).
[25] L. R. McCunn, M. J. Krisch, K. Takematsu, L. J. Butler, and J. Shu, J. Phys. Chem. A **108**, 7889 (2004).
[26] J. L. Miller, L. R. McCunn, M. J. Krisch, L. J. Butler, and J. Shu, J. Chem. Phys. **121**, 1830 (2004).
[27] L. A. Curtiss, K. Raghavachari, P. C. Redfern, V. Rassolov, and J. A. Pople, J. Chem. Phys. **109**, 7764 (1998).
[28] A. G. Baboul, L. A. Curtiss, P. C. Redfern, and K. Raghavachari, J. Chem. Phys. **110**, 7650 (1999).
[29] L. A. Curtiss, P. C. Redfern, K. Raghavachari, and J. A. Pople, J. Chem. Phys. **114**, 108 (2001).
[30] (a) N. L. Ma, K.-C. Lau, S.-H. Chien, and W.-K. Li, Chem. Phys. Lett. **311**, 275 (1999); (b) S.-H. Chien, K.-C. Lau, W.-K. Li, and C. Y. Ng, J. Phys. Chem. A **103**, 7918 (1999); (c) W.-K. Li, K.-C. Lau, C. Y. Ng, H. Baumgärtel, and K.-M. Weitzel, *ibid.* **104**, 3197 (1999).
[31] Y. Liu and L. J. Butler, J. Chem. Phys. **121**, 11016 (2004).
[32] S. Arepalli, N. Presser, D. Robie, and R. J. Gordon, Chem. Phys. Lett. **118**, 88 (1985).
[33] B.-Y. Chang, R. C. Hoetzlein, J. A. Mueller, J. D. Geisler, and P. L. Houston, Rev. Sci. Instrum. **69**, 1665 (1998).
[34] V. Dribinski, A. Ossadtchi, V. A. Mandelshtam, and H. Reisler, Rev. Sci. Instrum. **73**, 2634 (2002).
[35] (a) C. Hampel, K. A. Peterson, and H. Werner, Chem. Phys. Lett. **190**, 1 (1992); (b) M. J. O. Deegan and P. J. Knowles, *ibid.* **227**, 321 (1994); (c) P. J. Knowles, C. Hampel, and H. J. Werner, J. Chem. Phys. **99**, 5219 (1988).
[36] (a) T. H. Dunning, Jr., J. Chem. Phys. **90**, 1007 (1989); (b) T. H. Dunning, Jr., K. A. Peterson, and A. K. Wilson, *ibid.* **114**, 9244 (2001).
[37] K. A. Peterson and T. H. Dunning, Jr., J. Chem. Phys. **117**, 10548 (2002).
[38] M. J. Frisch, G. W. Trucks, H. B. Schlegel *et al.*, GAUSSIAN03, Revision B.05, Gaussian, Inc., Pittsburgh, PA, 2003.
[39] H.-J. Werner, P. J. Knowles, M. Schütz *et al.*, MOLPRO, a package of *ab initio* programs.
[40] M. L. Morton, L. J. Butler, T. A. Stephenson, and F. Qi, J. Chem. Phys. **116**, 2763 (2002).
[41] L. R. McCunn, D. I. G. Bennett, L. J. Butler, F. Aguirre, and S. T. Pratt, J. Phys. Chem. A (submitted).
[42] R. Liyanage, Y. A. Yang, S. Hashimoto, R. J. Gordon, and R. W. Field, J. Chem. Phys. **103**, 6811 (1995).
[43] Y. Matsumi, P. K. Das, M. Kawasaki, K. Tonokura, T. Ibuki, G. Inoue, S. Satyapal, and R. Bersohn, J. Chem. Phys. **97**, 5261 (1992).
[44] V. Skorokhodov, Y. Sato, K. Sato, Y. Matsumi, and M. Kawasaki, J. Phys. Chem. **100**, 12321 (1996).
[45] M. Ahmed, D. Blunt, D. Chen, and A. G. Suits, J. Chem. Phys. **106**, 7617 (1997).
[46] J. Zhang, M. Dulligan, and C. Wittig, J. Chem. Phys. **107**, 1403 (1997).
[47] A. L. Cooksy, J. Phys. Chem. A **102**, 5093 (1998).
[48] See EPAPS Document No. E-JCPSA6-123-032528 the EPAPs supplement contains the optimized geometries (in Angstroms), rotational constants (in GHz), the vibrational frequencies (in cm^{-1}) of the *trans-*/*cis-*/*linear*-CH_2CHCO radical, the *cis-*/*-trans*-transition state structures, and the CH_2CH and CO products at the CCSD(T)/6–311g(2df,p) level of theory. This document can be reached via a direct link in the online article's HTML reference section or via the EPAPS homepage (http://www.aip.org/pubservs/epaps.html).
[49] J.-H. Park, H. Lee, and J.-H. Choi, J. Chem. Phys. **119**, 8966 (2003).
[50] S.-K. Joo, L.-K. Kwon, H. Lee, and J.-H. Choi, J. Chem. Phys. **120**, 7976 (2004).
[51] J.-H. Park, H. Lee, H.-C. Kwon, H.-K. Kim, Y.-S. Choi, and J.-H. Choi, J. Chem. Phys. **117**, 2017 (2002).
[52] I. R. Slagle, J. R. Bernhardt, D. Gutman, M. A. Hanning-Lee, and M. J. Pilling, J. Phys. Chem. **94**, 3652 (1990).